FUDMA Journal of Sciences (FJS)
ISSN online: 2616-1370
ISSN print: 2645 - 2944
Vol. 8 No. 5, October, 2024, pp 210 - 223
DOI: https://doi.org/10.33003/fjs-2024-0805-2833

EFFECT OF RADIATION PRESSURE ON DYNAMICAL STRUCTURES IN THE CIRCULAR ROBE'S R3BP WITH VARIABLE MASSES

***Oni Leke and Masankari Clement**

Department of Mathematics, College of Physical Science, Joseph Sarwuan Tarka University, P.M.B. 2373, Makurdi, Benue-State Nigeria

*Corresponding authors' email: leke.o@uam.edu.ng

ABSTRACT

The paper investigates effect of radiation pressure on dynamical structures in the Robe's restricted three-body problem (R3BP) with variable masses. The non-autonomous equations of the dynamical system are obtained and transformed to the autonomized equations with constant coefficients under the condition that there is no fluid inside the first primary. Next, the equilibrium points (EPs) of the autonomized system are explored and the stability is investigated analytically and numerically. It is observed that the axial and non-collinear EPs can be stable and unstable depending on the values of the mass parameter, radiation pressure of the second primary and the mass variation parameter κ. In the case of the axial equilibrium point (EP), the radiation pressure reduces the region of stable motion while the mass variation parameter can have both stabilizing and destabilizing effects. The stability of the EPs of the non-autonomous equations is analyzed and it is seen that the solutions do not converge, and are unstable EPs. Finally, the ZVCs around the EPs are explored and it is seen that, the radiation pressure of the second primary decreases the region where motion of the satellite around the axial EP, is allowed, while the mass parameter and the parameter κ decreases or increases the region where motion of the satellite around the axial EP is allowed, as they are increased or decreased, respectively. In the case of the non-collinear points, the radiation of the second primary increases the region where motion of the satellite is allowed, while an increase in the mass parameter and mass variation parameter decreases the region where motion is allowed. The studied problem can be applied to small oscillation in the Earth's core of the Earth-Moon system with variable masses.

Keywords: Robe's R3BP, Stability, Zero velocity curves, Variable mass, Radiation pressure

INTRODUCTION

The restricted three-body problem (R3BP) is the most fascinating problem in celestial mechanics. This model illustrates motion of a third body having mass infinitesimally small and moving in the gravitational surrounding of two main masses, called primaries. The primaries move in circular orbits around their center of mass on account of their mutual attraction and the third body does not affect the motion of the primaries. Since no general solution in the R3BP is obtainable, particular solutions are required to obtain insight into the set up - These solutions are referred to as the equilibrium points (EPs) and five such solutions exists for the classical R3BP; two triangular equilibrium points (TEPs) and three collinear EPs (Szebehely 1967).

A variant form of the R3BP was formulated by Robe (1977). This problem was later called the Robe's Restricted Three Body Problem (RR3BP). In this formulation, the first body of mass m_1, is a rigid spherical shell, filled with homogenous, incompressible fluid of density ρ_1, with the second body as a small point outside the shell and moving around the first body in a Keplerian orbit. The third body is taken as a small sphere of densityρ_3, travelling inside the first body on account of the attraction of the second body and the buoyancy force due to the fluid. Further, the radius of the third body is assumed to be very negligible. Robe found an EP at the center of the shell and analyzed the linear stability in two cases. The first case examines the orbit of the second body around the first in circular while in the second case, the orbit is elliptical, but the shell is empty.

Shrivastava and Garain (1991) explored the impact of small deflective forces on the location of EP in the Robe's CR3BP with consideration that the densities of fluid and the third body are equal; in other words, the shell is empty. Plastino and Plastino (1995) studied the Robe's R3BP by considering the first body as a Roche spheroid in an equilibrium state of a rotational fluid and named the formulation the "Robe-Roche restricted model". The influence of small deflective forces on the location and stability of the EPs in the Robe's circular R3BP was reconsidered by Hallan and Rana (2001a), when the density of the more massive primary and that of the third body is equal. Further, the existence of all EPs, their location and stability in the Robe's (1977) R3BP when the densities of the fluid and the third body are not same, was studied by Hallan and Rana (2001b).

Singh and Sandah (2012) investigated the existence and linear stability of EPs in the Robe's R3BP with oblateness, while Singh and Laraba (2012) examined the Robe's CR3BP when the first body is a fluid in the shape of an oblate spheroid and the second one is a triaxial rigid body. The investigation of the Robe's problem of 2+2 bodies was carried out by Kaur and Aggarwal (2012) and the study was applied to dynamics of two submarines in the Earth-Moon system. Singh and Leke (2013b, c) investigated the Robes Problems when the masses are subject to mass variations while Singh and Omale (2014) studied the Robe's CR3BP with zonal harmonics. Ansari et. al (2019) explored the circular RR3BP with viscous force of the fluid effects of small perturbing forces in the Coriolis and centrifugal forces, while Abouelmagd et *al*. (2020) carried out a study on Robe's restricted problem with a modified Newtonian potential and emphasized that the model can be used to analyze the oscillations of the Earth's core under the influence of the Moon and it is also appropriate to study the dynamics of underwater vehicles. The effect of small perturbing forces in the Coriolis and centrifugal forces in the Robe-finite straight segment model with random density parameter was carried out by Kaur et. al (2020). Further, Kaur

et. al (2021), unveiled the outcomes of aspheric main bodies in Robe's R3BP, while Kaur and Kumar (2021) examined the stability investigation in the perturbed CRR3BP finite straight segment model under the influence of viscosity. A study on Robe's restricted problem with heterogeneous irregular primary of N-layers under the condition that the outer most layer has viscous fluid, was investigated by Ansari (2021), while, Ansari and Sahdev (2022) examined impact of a variable mass body motion in the perturbed Robe's model. Kaur et. al (2022), explored impacts of viscosity and oblateness on the perturbed Robe's problem with non-spherical bodies, while Leke and Ahile (2022) carried out a study on stability of EPs the Robe's R3BP under density variation.

The model of the classical R3BP specifies that the masses of bodies do not change with time. Nevertheless, the phenomenon of absorption in stars steered scientists to design the R3BP with variable mass (es). The R3BP with variable mass models is applicable in many astronomical and engineering designs, such as, investigating the motion of spacecraft in the vicinity of an asteroids or comets with variable masses due to surface out-gassing. Exploring motion of binary stars with mass transfer between them, and also studying motion in the Earth-Moon system during lunar mass expulsion.

The investigations of the R3BP in the case where mass variations of the primaries take place under the Mestschersky unified Law (MUL) and their motion described by the Gylden-Mestschersky problem (GMP) (Gylden, 1884, Mestschersky 1903), has been carried out by several authors under different characterizations. Among such authors are Gelf'gat (1973), Bekov (1988), Luk'yanov (1989), Singh and Leke (2010, 2012, 2013a, b, c,), Leke and Singh (2023), Leke and Mmaju (2023), Leke and Orum (2024).

Singh and Leke (2013b) discussed the Robe's R3BP with variable masses, in which mass variations occur in accordance with the MUL. They found an EP at the center, which is stable and a pair of EPs on the $\xi\zeta -$ plane which are unstable.

Motivated by this, the aim of this paper is to study the effect of radiation pressure on dynamical structures in the circular Robe's R3BP with variable masses. The paper is structured as follows: in Sect. 2, the dynamical equations of the systems with variable and constant coefficients are deduced and the EPs and their stability are explored. The results and discussion are given in Sect 3 while the conclusion is given in Sect.4 of the paper.

MATERIALS AND METHODS

Dynamical Equations

In this model formulation, we consider the second body as a radiating body. Therefore, the forces acting on m_3 are

i. The force of attraction of the radiating second primary, which is given by

$$\vec{F}_{m_2} = -\frac{Gm_2q_2m_3\bar{r}_{23}}{r_{23}^3}$$

ii. The force of gravitation $\vec{F}_A$ exerted by the fluid $\vec{F}_A = -\frac{4\pi G\Re^3 m_3 m\delta_1\vec{r}_{13}}{3r_{13}^3}$

iii The buoyancy force: $\vec{F}_B = -\frac{4G\pi\Re^3 m_3}{3r_{13}^3}\frac{\delta_1^2\vec{r}_{13}}{\delta_3}$

iv. Radiation pressure $q_2$of the second primary

where G is the gravitational constant, $\Re$is the radius of the fluid, $\delta_i(i=1,3)$ is the density of the fluid and the test particle, respectively, while $\bar{r}_{13}$and $\bar{r}_{23}$ is the radius vector of the line joining the centers of the first and second body to the test particle, respectively and q_2 is the radiation pressure factor of the second primary (See Figure 1)

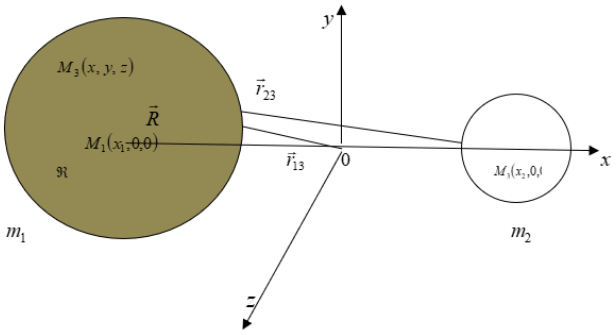

Figure 1: Set up of the Robe restricted three-body problem

variable masses in a Cartesian coordinate system, when the second primary is a radiation emitter, takes the form

$$\ddot{x} - 2\omega\dot{y} = \omega^2 x + \dot{\omega}y - \frac{4\pi\Re^3}{3}\frac{G\delta_1}{r_{13}^3}\left(1-\frac{\delta_1}{\delta_3}\right)(x-x_1) - \frac{\mu_2 q_2(x-x_2)}{r_{23}^3}$$

$$\ddot{y} + 2\omega\dot{x} = \omega^2 y - \dot{\omega}x - \frac{4\pi\Re^3}{3}\frac{G\delta_1 y}{r_{13}^3}\left(1-\frac{\delta_1}{\delta_3}\right) - \frac{\mu_2 q_2 y}{r_{23}^3} \quad (1)$$

$$\ddot{z} = -\frac{4\pi\Re^3}{3}\frac{G\delta_1 z}{r_{13}^3}\left(1-\frac{\delta_1}{\delta_3}\right) - \frac{\mu_2 q_2 z}{r_{23}^3}$$

where:$\mu(t) = \mu_1(t) + \mu_2(t)$:$\mu_1(t) = Gm_1, \mu_2(t) = Gm_1(t)$ $r_{13}^2 = (x-x_1)^2 + y^2 + z^2$, $r_{13}^2 = (x-x_2)^2 + y^2 + z^2$ and ω is the angular velocity of revolution of the primaries.

Now, system (2) is a non-autonomous system of equations and we have to transform it to the autonomized forms. However, it is impossible to carry out a complete transformation using the MT, the MUL, the particular solutions and integral of the GMP when the density parameter is not zero. In view of this, we restrict ourselves to the case when the first primary is empty.

In this premise, the system of equations (1) reduces to

$$\ddot{x} - 2\omega\dot{y} = \omega^2 x + \dot{\omega}y - \frac{\mu_2 q_2(x-x_2)}{r_{23}^3}$$

$$\ddot{y} + 2\omega\dot{x} = \omega^2 y - \dot{\omega}x - \frac{\mu_2 q_2 y}{r_{23}^3} \quad (2)$$

$$\ddot{z} = -\frac{\mu_2 q_2 z}{r_{23}^3}$$

$$r_{13}^2 = (x-x_2)^2 + y^2 + z^2$$

Equations (2) in the autonomized equations with constant coefficients is given as

$$\xi'' - 2\eta' = \frac{\partial\Omega}{\partial\xi}, \eta'' + 2\xi' = \frac{\partial\Omega}{\partial\eta}, \zeta'' = \frac{\partial\Omega}{\partial\zeta} \quad (3)$$

Where $\Omega = \frac{\kappa(\xi^2+\eta^2)}{2} + \frac{(\kappa-1)\zeta^2}{2} + \frac{\kappa\upsilon q_2}{\rho_{23}}$ (4)

$$\rho_{13}^2 = (\xi+\upsilon-1)^2 + \eta^2 + \zeta^2 \quad (5)$$

Where υ is the mass ratio and is such that $0 < \upsilon < 1$, while κ is the random sum of the masses of the main bodies in the autonomized system.
Equations (3) admits the Jacobian integral
$$2\Omega(\xi,\eta,\zeta) - \left(\xi'^2 + \eta'^2 + \zeta'^2\right) = C \qquad (6)$$

Locations and Stability of Equilibrium Points
The positions of the EPs can be obtained by solving the equations $\Omega_\xi = \Omega_\eta = \Omega_\zeta = 0$. That is, we will solve the system of equations

$$k\left[\xi - \frac{q_2\upsilon(\xi+\upsilon-1)}{[(\xi+\upsilon-1)^2+\eta^2+\zeta^2]^{\frac{3}{2}}}\right] = 0$$
$$k\eta\left[1 - \frac{q_2\upsilon}{[(\xi+\upsilon-1)^2+\eta^2+\zeta^2]^{\frac{3}{2}}}\right] = 0 \qquad (7)$$
$$\zeta\left\{(k-1) - \frac{q_2\kappa\upsilon}{[(\xi+\upsilon-1)^2+\eta^2+\zeta^2]^{\frac{3}{2}}}\right\} = 0$$

Locations of equilibrium points
Axial equilibrium point

i. The axial EP is the solution of equations (7) when $\eta = \zeta = 0$. Solving, we get

$$\xi = -\upsilon\left[1 - \frac{(1-q_2)}{1+2\upsilon}\right] \qquad (8)$$

This gives an EP on the line joining the centers of the first and second body away from the center of the first body but located inside it and is defined by the mass parameter and radiation factor of the second primary. When there is no radiation from the second body, the point fully coincides with that in Robe (1977), Hallan and Rana (2001a), and, Singh and Leke (2013b)

Non-collinear Equilibrium Points
The existence of the non-collinear equilibrium points (NCEPs) was not found in the Robe (1977) problem. The NCEPs of the autonomized equations are obtained by solving system (7), when $\eta = 0$, $\zeta \neq 0$ to get

$$\xi = -(1-\upsilon)(\kappa-1) \text{and} \zeta = \pm\sqrt{\left(\frac{q_2\kappa\upsilon}{k-1}\right)^{\frac{2}{3}} - \kappa^2(1-\upsilon)^2} \qquad (9)$$

Equations (9) give the position of four NCEPs $\xi, 0, \zeta$ which exist for $\kappa > 1$ and are located on the $\xi\zeta -$ plane. These points, depend on the mass ratio and a constant of mass variations and radiation pressure of the second primary.
For the non-autonomous system, the EP near the center of the shell and the NCEPs are sought using the MT. These points differ from those of the system of equations with constant coefficient only by the function $R(t)$. We express them as

$$x^{(1)}(t) = \xi^{(1)}R(t),\ x^{(2)}(t) = \xi^{(2)}R(t),$$
$$x^{(3)}(t) = \zeta^{(2,3)}R(t) \qquad (10)$$

where $x^{(1)}$ is the axial EP which varies with time while $x^{(2)}$ and $z^{(2,3)}$ are the NCEPs of the non-autonomous systems varying with time. $\xi^{(1)}$, and $\xi^{(2)}$, $\zeta^{(2,3)}$ are the axial and non-collinear EPs, of the autonomized system, respectively.

Stability of equilibrium points
The stability analysis of the EPs is same with that of the general R3BP of Szebehely (1967). We apply small displacement u, v and w to the coordinates (ξ_0, η_0, ζ_0) of the test body, to the locations, $\xi = \xi_0 + u$, $\eta = \eta_0 + v$ and $\zeta = \zeta_0 + w$ If its motion departs from the vicinity of the point, such a position is an unstable one. However, if it oscillates about the point, then it is a stable position.

The variational equations in this case, are:
$$u'' - 2v' = \left(\Omega^0_{\xi\xi}\right)u + \left(\Omega^0_{\xi\eta}\right)v + \left(\Omega^0_{\xi\zeta}\right)w$$
$$v'' + 2u' = \left(\Omega^0_{\xi\eta}\right)u + \left(\Omega^0_{\eta\eta}\right)v + \left(\Omega^0_{\eta\zeta}\right)w \qquad (11)$$
$$w'' = \left(\Omega^0_{\xi\zeta}\right)u + \left(\Omega^0_{\eta\zeta}\right)v + \left(\Omega^0_{\zeta\zeta}\right)w$$
The superscript 0 depicts that the partial derivatives are to be computed at the EPs.

Axial Equilibrium Point
In order to analyze the stability of the axial EP we obtain the characteristic equation which corresponds to the first two equations of the variational equations (11):
$$\lambda^4 - \left(\Omega^0_{\xi\xi} + \Omega^0_{\eta\eta} - 4\right)\lambda^2 + \Omega^0_{\xi\xi}\Omega^0_{\eta\eta} - \left(\Omega^0_{\xi\eta}\right)^2 = 0 \qquad (12)$$
where
$$\Omega^0_{\xi\xi} = \kappa + 2\kappa\upsilon[1 + 3p - (1-q_2)]$$
$$\Omega^0_{\eta\eta} = \kappa - \kappa\upsilon[1 + 3p - (1-q_2)] \qquad (13)$$
$$\Omega^0_{\zeta\zeta} = \kappa - 1 - \kappa\upsilon[1 + 3p - (1-q_2)],$$
$$\Omega^0_{\xi\zeta} = \Omega^0_{\eta\zeta} = \Omega^0_{\xi\eta} = 0$$
$p = \frac{\upsilon(1-q_2)}{1+2\upsilon}$, $p << 1$since $1 - q_2 << 1$and $p = 0$when $q_2 = 1$
Now, substituting the partial derivatives into the variational equations of motion (11), we get
$$u'' - 2v' = [\kappa(1+2\upsilon) + 6p\kappa\upsilon - 2\kappa\upsilon(1-q_2)]u$$
$$v'' + 2u' = [\kappa(1-\upsilon) - 3p\kappa\upsilon + \kappa\upsilon(1-q_2)]v \qquad (14)$$
$$w'' = [\kappa(1-\upsilon) - 1 - 3p\kappa\upsilon + \kappa\upsilon(1-q_2)]w$$
The third equation of (14) is independent of the first two equations and shows that motion parallel to the $\zeta -$axis is stable when $1 \leq \kappa < \frac{1}{(1-3p\upsilon-q_2\upsilon)}$, otherwise it is unstable. When the second primary is a non-radiating body, we have $q_2 = 1$and$p = 0$. In this case, motion is stable in the $\zeta -$axis when $1 \leq \kappa < \frac{1}{(1-\upsilon)}$, which coincides with that given in Singh and Leke (2013b).
Now, substituting equations (13) in the characteristic equation (12), we have
$$\lambda^4 + P\lambda^2 + Q = 0 \qquad (15)$$
where
$$P = 4 - \kappa(2+\upsilon) - 3p\kappa\upsilon + \kappa\upsilon(1-q_2)$$
$$Q = \kappa^2[(1 + \upsilon - 2\upsilon^2) + p\upsilon(3 - 12\upsilon) - \upsilon(1-4\upsilon)(1-q_2)]$$
Evidently, $Q > 0$, while $P <=> 0$ when $\kappa <=> \frac{4}{[2+\upsilon+3p\upsilon-\upsilon(1-q_2)]}$, respectively.
The roots are
$$\lambda^2_{1,2} = \frac{-[4 - \kappa(2+\upsilon) - 3p\kappa\upsilon + \kappa\upsilon(1-q_2)] \pm \sqrt{D}}{2}$$
where
$$D = -16(\kappa-1) + \kappa\upsilon(9\kappa\upsilon - 8) - 6p\kappa\upsilon(4 - 9\kappa\upsilon) + 2\kappa\upsilon(4 - 9\kappa\upsilon)(1-q_2) \qquad (16)$$
is the discriminant of the equation (15).
When the second primary is not a radiation source, we have
$D = -16(\kappa-1) + \kappa\upsilon(9\kappa\upsilon - 8)$
This coincides with that obtained by Singh and Leke (2013b)
Solving equation (16) for υ when the discriminant vanishes to obtain the critical mass parameter, given
$$\upsilon_{C\kappa} = \frac{4}{9\kappa}\left[1 + \sqrt{(9\kappa-8)[1+2(1-q_2)]} + (1-q_2)\right] \qquad (17)$$
Equation (17) are the values of the critical mass parameter which exists for various values of the mass variation parameter, and the radiation of the second body. When the second body is not a source of radiation, that is $q_2 = 1$, the critical mass reduces to that in Singh and Leke (2013b). Further, when $\kappa = 1$ (that is when mass variations are ignored), the critical mass reduces to that obtained by Robe

(1977), Hallan and Rana (2001a). The values of the critical mass values exists for $\kappa \geq \frac{8}{9}$

Now, from equation (16), we have

$$\frac{dD}{dv} = 18\kappa^2 v - 8\kappa - 24p\kappa + 108p\kappa^2 v - 36\kappa^2 v(1-q_2) \quad (18)$$

Also, $\frac{dD}{dv} = 0$, when

$$v = \frac{4(1+3p)}{9\kappa[1+6p-2(1-q_2)]} \quad (19)$$

When $q_2 = 1$, we have $p = 0$ and we get $v = \frac{4}{9\kappa}$ which coincides with that in Singh and Leke (2013b).

Therefore, equation (18) is positive when $v > \frac{4(1+3p)}{9\kappa[1+6p-2(1-q_2)]}$ and negative when $v < \frac{4(1+3p)}{9\kappa[1+6p-2(1-q_2)]}$.

This implies that D is strictly increasing when the former holds and strictly decreasing when the later is the case.

Next,-when $v = 0$in Equation (16), we have

$$D = -16(\kappa - 1) \quad (20)$$

However, when$v = \frac{4(1+3p)}{9\kappa[1+6p-2(1-q_2)]}$, equation (28) reduces to

$$D = -\frac{16(9\kappa-10)}{9} \quad (21)$$

We observe that equation (21) is negative in sign when $\kappa \geq \frac{10}{9}$. Further, as v increases to $v_{c\kappa}$, D increases from the value in (21) to zero. Finally, $v_{c\kappa}$ increases to 1, when D increases from 0 to

$$D = \kappa^2[9 + 54p - 18(1-q_2)] - \kappa[24 + 24p - 8(1-q_2)] + 16 \quad (22)$$

A careful inspection of equation (22) shows that for $0 < \kappa < \infty$, we have $D > 0$.

Now, since the natures of the roots depend on the discriminant, the mass parameter, $\kappa$and radiation factor of the second primary; we see that when $v_{c\kappa} < v < 1$. D is positive. Hence, when$\kappa < \frac{4}{[2+v+3pv-v(1-q_2)]}$, the characteristic roots are all distinct pure imaginary. In this case, the axial point is stable, otherwise it will be unstable.

We shall numerically explore the kinds of the roots of the characteristic equation and the critical mass parameters.

Non-collinear Equilibrium Points

We follow same procedure done for the axial EP. Therefore, we obtain the characteristic equation of the NCEPs:

$$\lambda^6 - c_1\lambda^4 + c_2\lambda^2 - c_3 = 0 \quad (23)$$

Where

$$c_1 = 3k - 5$$

$$c_2 = 7 - 6\kappa - \frac{9\kappa^2(\kappa-1)^4(1-v)^6}{v^2} + \frac{9\kappa^{7/3}(k-1)^{5/3}(1-v)^2}{v^{2/3}} - \frac{9\kappa^{8/3}(k-1)^{13/3}(1-v)^4}{v^{4/3}} + \frac{18\kappa^{4/3}(\kappa-1)^{10/3}(1-v)^4}{v^{7/3}} + \left[\frac{6\kappa^{7/3}(k-1)^{5/3}(1-v)^2}{v^{2/3}} - \frac{12\kappa^{8/3}(k-1)^{13/3}(1-v)^4}{v^{4/3}} + \frac{6\kappa^{4/3}(\kappa-1)^{10/3}(1-v)^4}{v^{7/3}}\right](1-q_2)$$

$$c_3 = 3 - 3k + \frac{3\kappa^{4/3}(k-1)^{5/3}(1-v)^2}{v^{2/3}} + \frac{6\kappa^{4/3}(k-1)^{5/3}(1-v)^2(1-q_2)}{3v^{2/3}}$$

These roots depend on the values of the coefficients, $c_i(i = 1,2,3)$ and shall be explored numerically to ascertain the kinds and the stability outcome.

In the case of the stability of the EPs of the non-autonomous system given in equation (10), we adopt the definition of a Lyapunov stable solution (Krasnov*et al.* 1983), to get

$$\lim_{t\to\infty} x^{(1)} = \xi^{(1)} \lim_{t\to\infty} R(t) = \infty \quad (24)$$

Equation (24) at once proves the instability of the axial EP $x^{(1)}(t)$ according to the Lyapunov's theorem. Same technique shows that the non-collinear EPs of the non-autonomous system are unstable.

RESULTS AND DISCUSSION

In this section, we study the numerical results of the analytical solutions that have been obtained in the paper. We shall consider the third body to be an artificial satellite in the gravitational environment of two main bodies. We carry out all numerical exploration with the aid of the software *Mathematica* (Wolfram 2015). Throughout, we select the radiation pressure of the second primary to be $\boldsymbol{q_2 = 0.99996.}$

Zero Velocity Curves around Axial Equilibrium Point

The Jacobi integral is given in Equation (6), where$V = \xi'^2 + \eta'^2 + \zeta'^2$is the velocity of the satellite and C is the Jacobi or energy constant. The permissible region of motion and prohibited region are defined by $V \geq 0$ and $V < 0$, respectively. Therefore, when the velocity of the satellite is zero, the curve shown by equation (6) is called zero-velocity curves (ZVCs) on the plane.. ZVC are important because they form the boundary of regions where the satellite is dynamically prohibited. The regions from which motion of the satellite is prohibited increases in area as the Jacobi constant grows, and vice versa.

For any given value of C, we can measure the impact of radiation pressure of the second primary, the mass ratio and the mass variation constant on the ZVCs of the Robe's circularR3BP with variable masses of the primaries. We now explore the ZVCs around the axial EP which have been given in Figures 2 to 4 under effects of the perturbing forces. These figures show for different values of the energy constant how the area from which the satellite is dynamically restricted and evolves as the value of the energy constant under radiation pressure of the second primary, mass parameter and mass variation parameter are changing. Any point not in the prohibited region is in the permissible area.

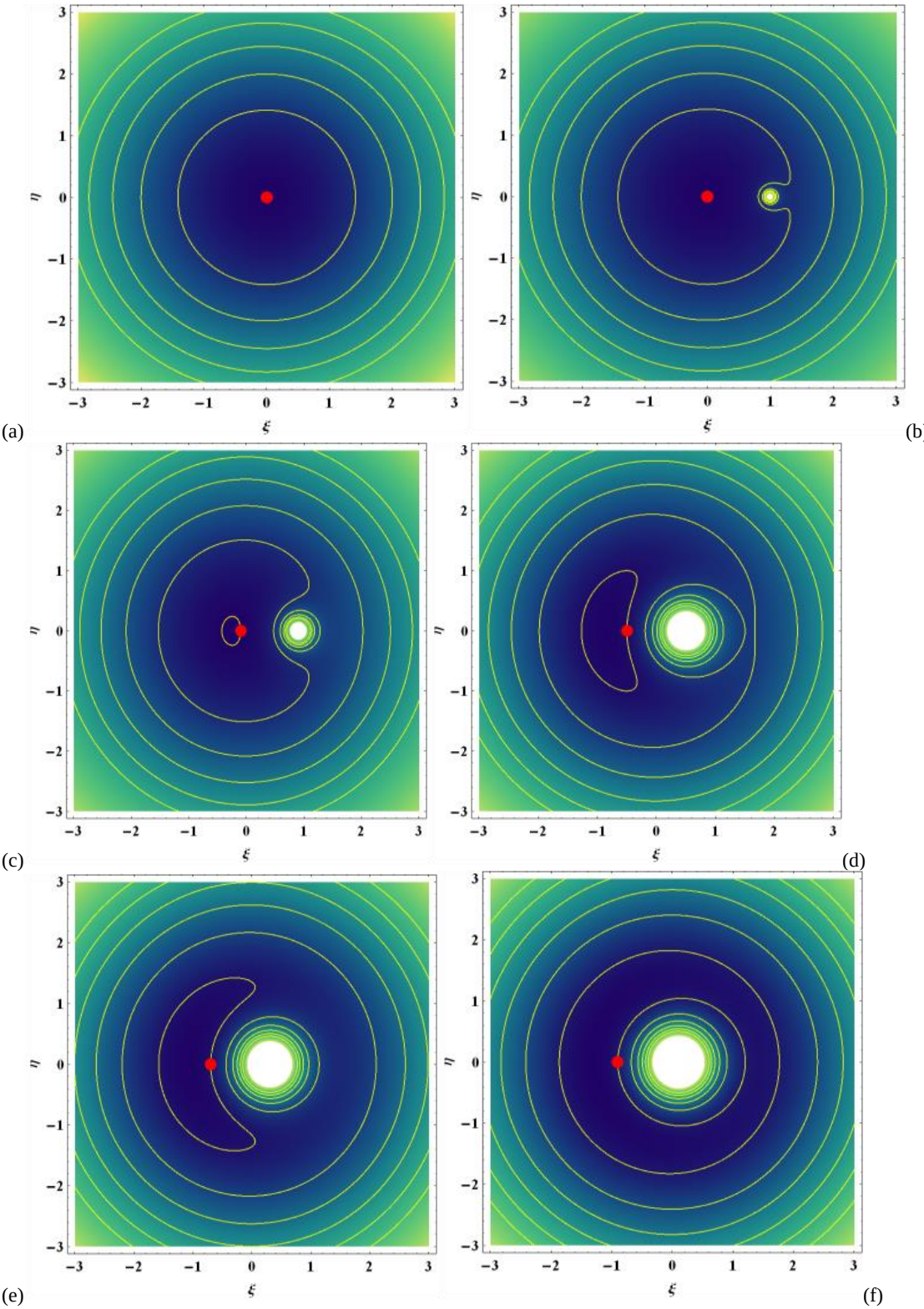

Figure 2: ZVCs when $\kappa = 0.1, q_2 = 0.99996$ and (a) $\upsilon = 0.000000001 \& C = 0.00000000039998$ (b) $\upsilon = 0.012 \& C = 0.00481421$ (c) $\upsilon = 0.1 \& C = 0.0409986$ (d) $\upsilon = 0.5 \& C = 0.224995$ (e) $\upsilon = 0.7 \& C = 0.328994$ (f) $\upsilon = 0.9 \& C = 0.440993$

The ZVCs around the axial EP have been plotted in Figure 2 for $\kappa = 0.1$ under the influence of radiation pressure of the second body when the mass parameters is varied in the interval $0 < \upsilon < 1$. Figure 2, panel "a" is the ZVCs when $\upsilon = 0.000000001$ and the energy constant is $C = 0.00000000039998$. Because the mass parameter which also is the mass of the second body is very small, the second body is completely overwhelmed by the first primary and the radiation effect is insignificant. In this case, the area where motion of the satellite is allowed-grows around the axial point. Figure 2 panel "b", shows the ZVCs around axial EPs when $\upsilon = 0.012$. It is seen that the second primary becomes visible

but the area where motion is allowed keeps reducing around the axial EP, due to the combined influence of the mass parameter and the radiation pressure. These region decreases with increase in the mass parameter as seen in Figure 2b to Figure 2d. In Figure 2e and Figure 2f, the mass of the second primary is large enough to the point that the second primary moves so close to the axial EP. However, the axial EP lies in the environment where motion of the satellite is not permitted. Therefore, we conclude that, the environment where motion of the satellite is permitted reduces with increasing mass parameter whether in the presence or absence of the radiation pressure of the second body or the mass variation constant. Also, it is observed that as the mass parameter increases the location of the axial EP is altered. The effects of the variable mass parameter on the ZVCs have been drawn in Figure 3a-f, under radiation pressure of the second primary.

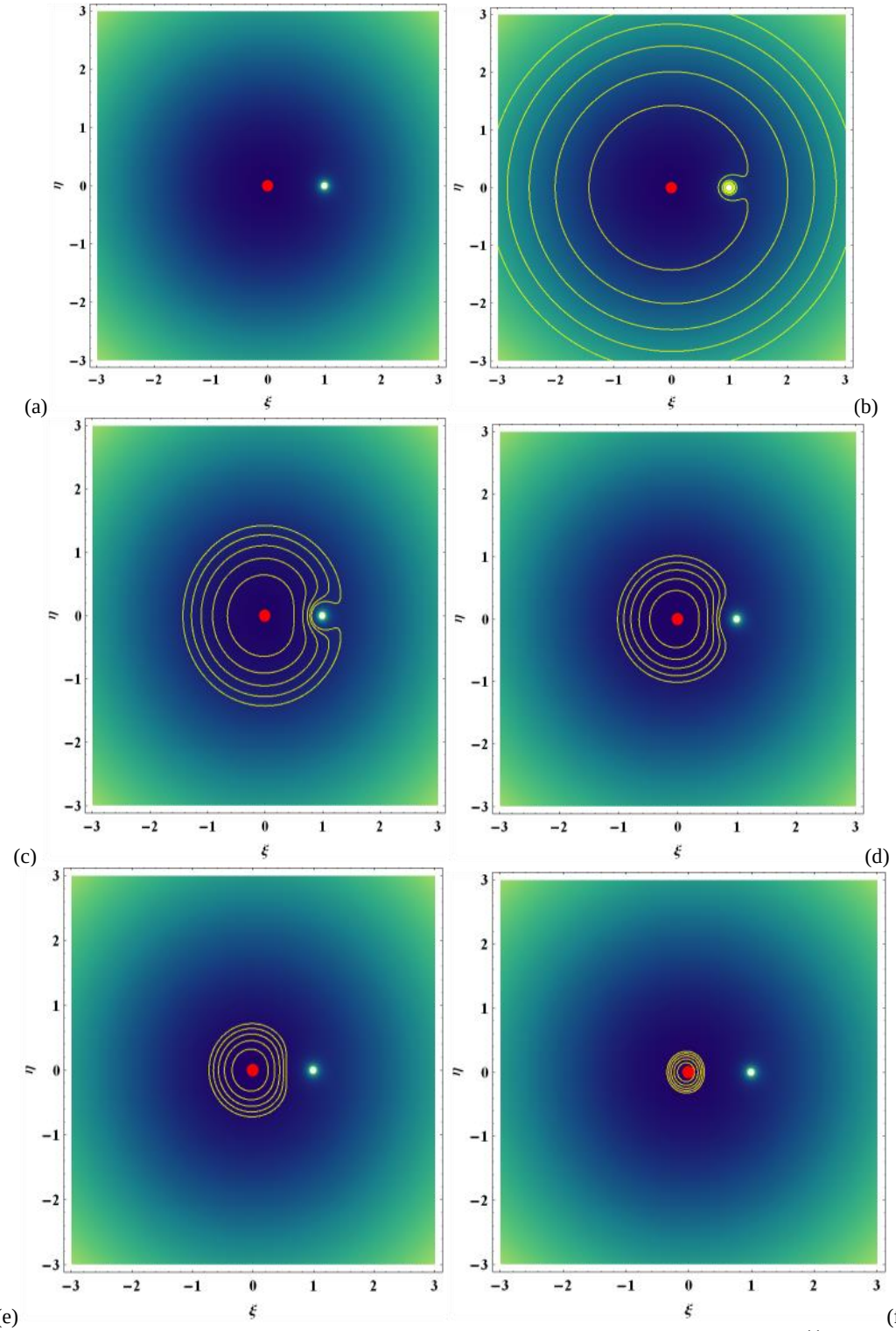

Figure 3: ZVCs for $\upsilon = 0.012$ and $q_2 = 0.99996$ when (a) $\kappa = 0.000000001$, $C = 4.81421 \times 10^{-11}$ (b) $\kappa = 0.1$, $C = 0.00481421$ (c) $\kappa = 0.5$, $C = 0.0240711$ (d) $\kappa = 1$, $C = 0.0481421$ (e) $\kappa = 2$, $C = 0.0962842$ (f) $\kappa = 10$, $C = 0.481421$

It is seen from Figure 3a-f, that when the variation constant increases, this leads to a reduction in the area where motion of the satellite is permitted around the axial EP, and vice versa. Hence, the variable mass parameter κ reduces or increases the area where motion is allowed whenever, it is increasing or decreasing, respectively.

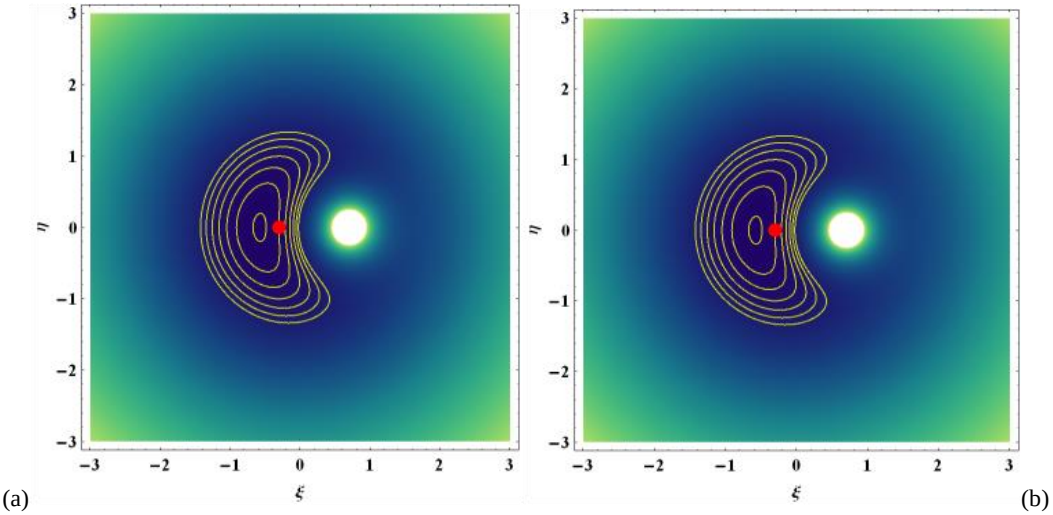

Figure 4: ZVCs when (a) $\upsilon = 0.3$, $\kappa = 1$, $q_2 = 0.99996$ and $C = 1.28996$ (b) $\upsilon = 0.3$, $\kappa = 1$, $q_2 = 1$ and $C = 1.29$ (c) $\upsilon = 0.012$(red) &$\upsilon = 0.9$(Green), for $q_2 = 0.99996$

Finally, Figure 4**a, b** illustrates the effect of the radiation pressure of the second body on the ZVCs while Figure 4c, shows the variations of the mass parameter when $\upsilon = 0.012$(red) and $\upsilon = 0.9$(Green), under effects of radiation pressure of the second primary. It is seen that the presence of the radiation pressure of the second primary reduces area where motion of the satellite is permitted, though the effect may be minimal. Also, from Figure 4c, it is seen the motion around the axial point designated in green ($\upsilon = 0.9$) is not allowed while it is allowed around the axial EP designated in red ($\upsilon = 0.012$).

We observe from our results, that when$0 < \upsilon < 1$, the area where motion of the satellite is allowed remain increasingly large for $0 < \kappa < 0.1$. However, this region begins to decrease when $\kappa = 0.1$. Hence, we conclude that the mass parameter and the mass variation parameter can increase or decrease the environment where motion of the satellite is permitted while the radiation pressure of the second primary always decreases the region of motion. Consequently, the mass parameter $\upsilon$and the variable mass parameter κcan have both stabilizing and destabilizing behaviors on the motion of the satellite around axial EP, while the radiation of the second primary $q_2$is always a destabilizing force.

Stability Analysis of the Axial Equilibrium Point

We now numerically compute the roots of the characteristic equation (15) in Table 1 to 4 for various values of the mass parameter and the parameter of mass variations when $q_2 = 0.99996$.

Table 1: Characteristic Roots and Critical Mass Parameter for $\upsilon = 0.012$ and $0 < \kappa < \infty$

κ	$\pm\omega_1$	$\pm\omega_2$	$\upsilon_{C\kappa}$
0.000000001	5.02919*10^-10i	2i	-1.33346*10^9
0.00001	5.02921*10^-6i	1.99999i	-133344.
0.01	0.00504191i	1.99496i	-131.346
0.1	0.0516247i	1.94837i	-11.3344
0.5	0.294969i	1.70499i	-0.666756
0.8	0.55808i	1.44186i	0.333338
0.9	0.692275i	1.30765i	0.51854
0.994	0.989177i	1.01074i	0.658653
0.995	Complex	Complex	0.660001
0.9999	Complex	Complex	0.666569
1	Complex	Complex	0.666702
2	Complex	Complex	1.33343
5	Complex	Complex	1.73347
10	Complex	Complex	1.86681
50	Complex	Complex	1.97349
100	Complex	Complex	1.98683
1000	Complex	Complex	1.99883
$\kappa \to \infty$	Real	Real	2.00016

Table 2: Characteristic Roots and Critical Mass Parameter for $\upsilon = 0.3$ and $0 < \kappa < \infty$

κ	$\pm\omega_1$	$\pm\omega_2$	$\upsilon_{C\kappa}$
0.000000001	Imaginary	Imaginary	-1.33346*10^9
0.00001	Imaginary	Imaginary	- 133344.
0.01	Imaginary	Imaginary	-131.346
0.1	Imaginary	Imaginary	-11.3344
0.5	Imaginary	Imaginary	-0.666756
0.8	Imaginary	Imaginary	0.333338
0.9	Imaginary	Imaginary	0.51854
0.994	Complex	Complex	0.658653
0.995	Complex	Complex	0.660001
0.9999	Complex	Complex	0.666569
1	Complex	Complex	0.666702
2	Complex	Complex	1.33343
5	Complex	Complex	1.73347
10	Complex	Complex	1.86681
50	Real	Real	1.97349
100	Real	Real	1.98683
1000	Real	Real	1.99883
$\kappa \to \infty$	Real	Real	2.00016

Table 3: Characteristic Roots and Critical Mass Parameter for $\upsilon = 0.7$ and $0 < \kappa < \infty$

κ	$\pm\omega_1$	$\pm\omega_2$	$\upsilon_{C\kappa}$
0.000000001	Imaginary	Imaginary	-1.33346*10^9
0.00001	Imaginary	Imaginary	-133344.
0.01	Imaginary	Imaginary	-131.346
0.1	Imaginary	Imaginary	-11.3344
0.5	Imaginary	Imaginary	-0.666756
0.8	Imaginary	Imaginary	0.333338
0.9	Imaginary	Imaginary	0.51854
0.994	Complex	Complex	0.658653
0.995	Complex	Complex	0.660001
0.9999	Complex	Complex	0.666569
1	Complex	Complex	0.666702
2	Complex	Complex	1.33343
3	Complex	Complex	1.55567
5	Real	Real	1.73347
10	Real	Real	1.86681
50	Real	Real	1.97349
100	Real	Real	1.98683

1000	Real	Real	1.99883
$\kappa \to \infty$	Real	Real	2.00016

Table 4: Characteristic Roots and Critical Mass Parameter for$\upsilon = 0.9999$and $0 < \kappa < \infty$

κ	$\pm\omega_1$	$\pm\omega_2$	$\upsilon_{C\kappa}$
0.000000001	Imaginary	Imaginary	-1.33346*10^9
0.00001	Imaginary	Imaginary	-133344.
0.01	Imaginary	Imaginary	-131.346
0.1	Imaginary	Imaginary	-11.3344
0.5	Imaginary	Imaginary	-0.666756
0.8	Imaginary	Imaginary	0.333338
0.9	Imaginary	Imaginary	0.51854
0.994	Imaginary	Imaginary	0.658653
0.995	Imaginary	Imaginary	0.660001
0.9999	Imaginary	Imaginary	0.666569
1	Imaginary	Imaginary	0.666702
2	Real	Real	1.33343
3	Real	Real	1.55567
5	Real	Real	1.73347
10	Real	Real	1.86681
50	Real	Real	1.97349
100	Real	Real	1.98683
1000	Real	Real	1.99883
$\kappa \to \infty$	Real	Real	2.00016

Table 1 to 4 give the roots and the values of the critical mass parameter (17) corresponding to the axial EP, for different values of the mass variation parameter and the mass ratio. We observe from Table 1, that when $\upsilon = 0.012$, the four roots are distinctive wholly imaginary roots when $0 < \kappa \leq 0.994$but are however complex when $0.995 \leq \kappa \leq 1000$. These four roots then become real when $\kappa \to \infty$. From Table 2, it is observed that the roots are imaginary when $0 < \kappa \leq 0.9$and are complex $0.994 \leq \kappa \leq 10$. These roots then become real as $\kappa \to \infty$. Table 3is the case when $\upsilon = 0.7$and the same trend of change in the nature of the roots is similar to that observed in Table 3. Finally, Table 4 gives the roots of the characteristic equation (15) when the mass parameter is $\upsilon = 0.9999$and $0 < \kappa < \infty$. In this case, the roots are imaginary different roots when $0 < \kappa \leq 1$ and then evolve into real roots when$1 < \kappa < \infty$. From Table 1 to 4, the values of the critical mass are negative because $\kappa \leq \frac{8}{9}$ and so they do not exists. Also, the value of the critical mass should not exceed one since we have $0 < \upsilon < 1$. Therefore, any value of the critical mass exceeding one is ignored and taken not to exists. Clearly, ii is seen that numerically when $\kappa < \frac{4}{[2+\upsilon+3p\upsilon-\upsilon(1-q_2)]}$, the roots are imaginary roots. For instance, in the case when $\upsilon = 0.9999$, we get $\kappa < 1.33338$, which holds according to Table 4 as all the roots when $\kappa < 1.33338$are all pure imaginary quantities. When $\kappa > 1.33338$, the roots are real . Therefore, the axial EP is stable when simultaneously the roots of the characteristic equation are distinct pure imaginary roots and when the critical mass, is less than the mass ratio. Hence, the axial EP can be unstable and stable depending on the radiation pressure of the second primary, mass parameter and the mass variation constant.

Zero Velocity Curves around the Non-Collinear Equilibrium Points

Equations (9) give the positions of a pair of Eps $\xi, 0, \zeta$ which exist for $\kappa > 1$ and lies in the $\xi\zeta -$plane. We call these points, non-collinear EPs and they depend on the mass ratio and the constant of mass variations and radiation pressure of the second primary. The locations of the NCEPs have been computed numerically in Table 5 to Table 12 using equation (9). We have indicated under the remark column whether the points exist or do not exists. The remark that they exist means the points are located inside the first primary, while they do not exist when the points are located outside the first primary. The ZVCs around the NCEPs have been explored and drawn in Figure 5 to Figure 8 for different values of the mass parameter and the parameterκ under effect of the radiation of the second primary.

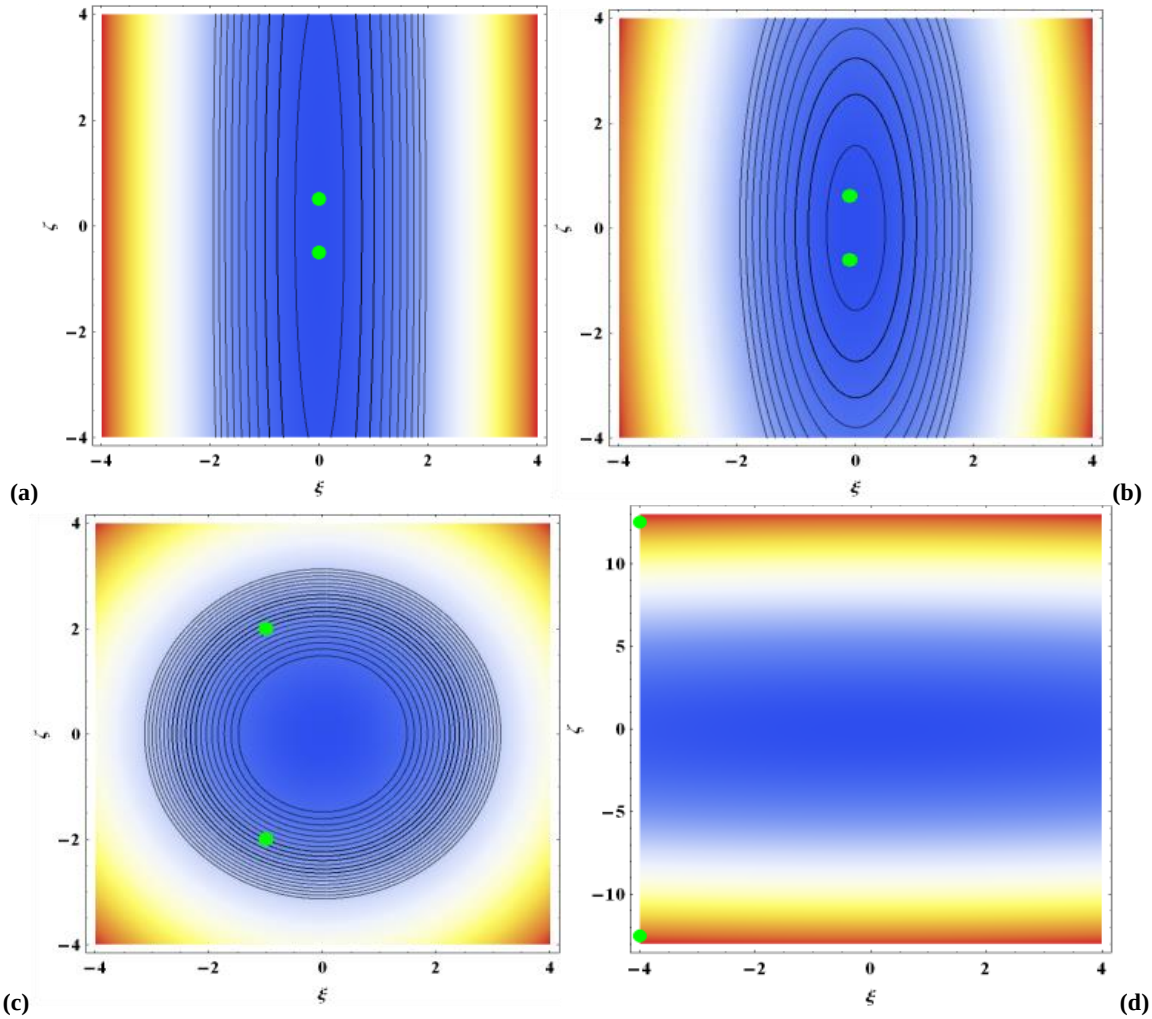

Figure 5: ZVCs of Non-collinear EPs for $\upsilon = 0.000000001$, $q_2 = 0.99996$ when(a) $\kappa = 1.01$ and $C = 0.002702$ (b) $\kappa = 1.1$and $C = 0.04760$(c) $\kappa = 2$and $C = 6$(d)$\kappa = 5$, $C = 705$

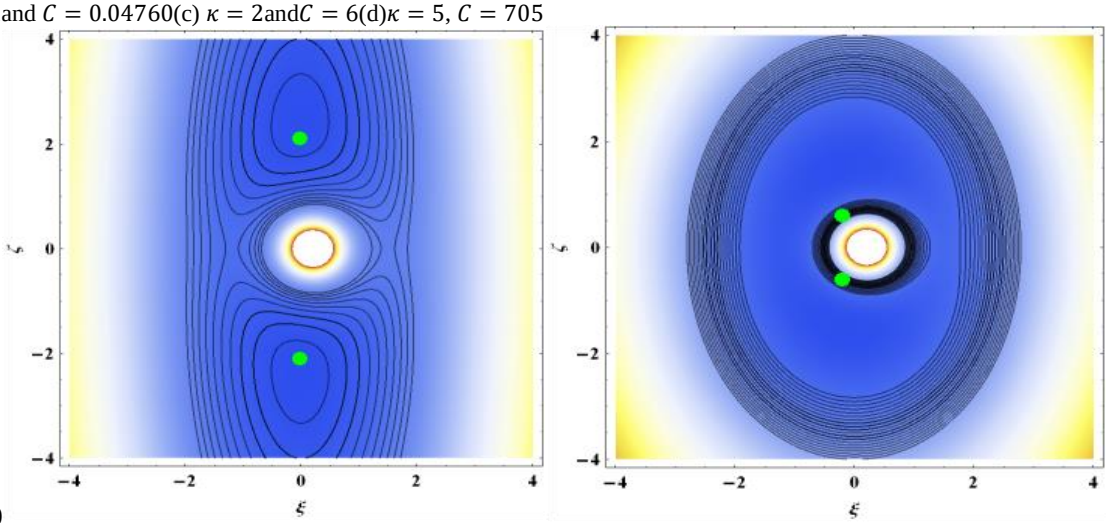

Figure 6: ZVCs of the Non-collinear EPs for $\upsilon = 0.8$and $q_2 = 0.99996$ when (a) $\kappa = 1.1$and $C = 1.22871$(b) $\kappa = 2$and $C = 12.6398$

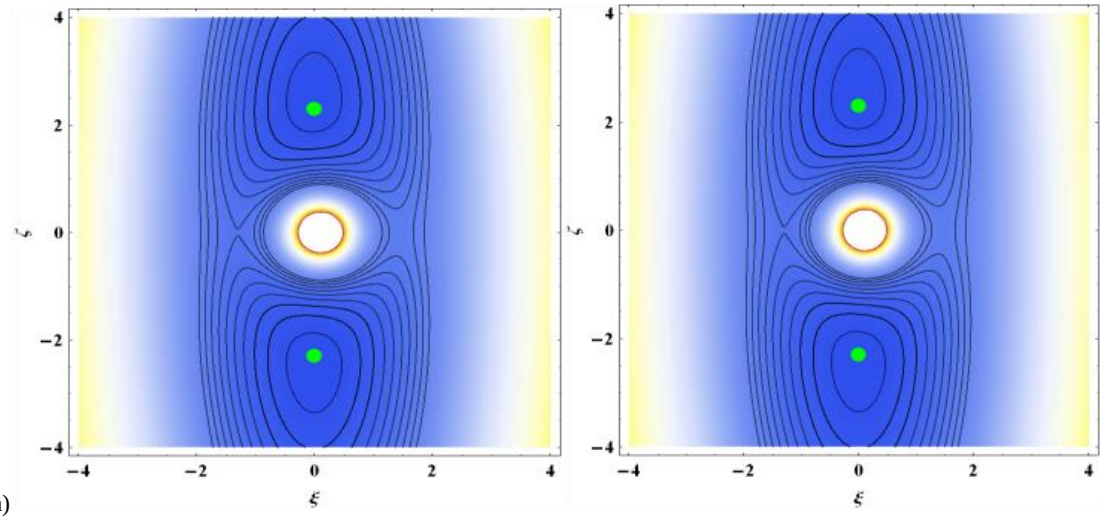

(a) (b)

Figure 7: ZVCs of the Non-collinear EPs for $\upsilon = 0.9$ and $\kappa = 1.1$when (a), $q_2 = 1$ and $C = 1.27613$(b) $q_2 = 0.99996$and $C = 1.27611$

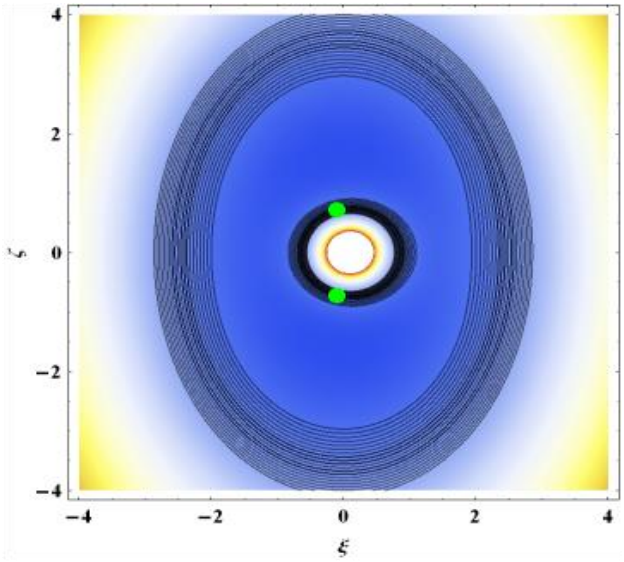

Figure 8: ZVCs of the Non-collinear EPs for $\upsilon = 0.9$, $q_2 = 0.99996$, $C = 13.4368$and $\kappa = 2$

Figure 5a-d gives the ZVCs of the NCEPs for $\upsilon = 0.000000001$, $q_2 = 0.99996$, and $\kappa = 1.01$, $\kappa = 1.1$, $\kappa = 2$and $\kappa = 5$, respectively. It is seen from Figure 5a, that when $\kappa = 1.01$, the energy constant is $C = 0.0027024$and the area where motion of the satellite increases but as the mass variation constant increases to 1.1 (Figure 5b), the energy constant also increases to $C = 0.0476023$and the area where motion of the satellite is permitted begins to decrease and decreases further in Figure 5c when $\kappa = 2$. In this case, motion near the NCEPs is not possible as they are located in the prohibited regions. The area where motion of the satellite is allowed soon disappears when $\kappa = 5$and $C = 705$ (Figure 5d), confirming that these points do not exists when $\upsilon = 0.000000001$ and $\kappa = 5$. Hence, motion of the satellite around the NCEPs when the mass ratio is very small and $\kappa \geq 5$is not possible as the region of motion do not exist since the positions of the NCEPs are located outside the first primary.

In Figure 6a, the ZVCs around the NCEPs is drawn for $\upsilon = 0.8$, $q_2 = 0.99996$, and $\kappa = 1.1$, thus yielding $C = 1.22871$. In this case the environment where motion of the satellite is permitted around the NCEPs grows for $\kappa = 1.1$but as kappa increases to 2 in Figure 6b, we observe that the environment where motion of the Earth's satellite is allowed decreases. However, the motion is possible around the non-collinear EPs. Therefore, an increase in the parameter kappa yields a reduction in the environment where motion of the satellite around the NCEPs is allowed.

Figure 7a is drawn when $\upsilon = 0.9$and $\kappa = 1.1$when the second primary is not a radiation emitter. Here we get $C = 1.27613$compared to Figure 7b where $C = 1.27611$when the radiation pressure of the second primary is present. Consequently, the region of motion increases slightly due to the presence of the radiation pressure of the second primary. Hence, we can conclude that the radiation pressure of the second body increases area where motion of the Earth's satellite is permitted around the NCEPs. Figure 7b is similar to Figure 6a, with the difference being the value of the mass parameter. When $\upsilon = 0.8$ and $\kappa = 1.1$, we have $C = 1.22871$ while when $\upsilon = 0.9$ and $\kappa = 1.1$ under radiation effect of the second primary, we get $C = 1.27611$. It is seen that increasing mass parameter yields a larger value of the energy constant and consequently, the area where motion of the satellite is permitted decreases with increase in the mass parameter. Figure 8 is similar to Figure 6b with the difference being the mass parameter. It is seen from Figure 6b that as the mass parameter increases from 0.8 to 0.9 in Figure 8, the

Jacobi constant also increases and the area where motion of the satellite is permitted decreases as seen when Figure 6b and Figure 8 are compared.

Stability of the Non-Collinear Equilibrium Points

We computed the partial derivatives and substituted in the variational equations of motion to obtain the characteristic equation (23). The six roots have been explored numerically to determine the kinds of roots in Table 5 to Table 8 for the mass ratios $\upsilon = 0.012$. $\upsilon = 0.3$, $\upsilon = 0.7$ and $\upsilon = 0.9999$, respectively, when $1 < \kappa < \infty$. Clearly, the kinds of roots will depend on the values of the coefficients, $c_i (i = 1,2,3)$in (23).

Table 5: Characteristic Roots of the Non-collinear EPs when$\upsilon = 0.012$and $1 < \kappa < \infty$

κ	$\pm\omega_1$	$\pm\omega_2$	$\pm\omega_3$
1.000000001	0.0000547717i	0.999961i	1.00004i
1.00001	0.00545382i	0.996138i	1.00382i
1.01	Complex	complex	imaginary
1.1	Complex	complex	Real
2	Complex	complex	Real
5	Imaginary	Imaginary	Real
10	Imaginary	Imaginary	Real
20	Imaginary	Imaginary	Real
50	Imaginary	Imaginary	Real
100	Imaginary	Imaginary	Real
1000	Imaginary	Imaginary	Real
$\kappa \to \infty$	Imaginary	Imaginary	Real

Table 6: Characteristic Roots of the Non-collinear EPs when$\upsilon = 0.3$and $1 < \kappa < \infty$

κ	$\pm\omega_1$	$\pm\omega_2$	$\pm\omega_3$
1.000000001	0.0000547722i	0.999961i	1.00004i
1.00001	0.00547616i	0.996106i	1.00385i
1.01	0.179604i	0.855053i	1.09847i
1.1	Complex	Complex	Imaginary
2	Complex	Complex	Real
5	Imaginary	Imaginary	Real
10	Imaginary	Imaginary	Real
20	Imaginary	Imaginary	Real
50	Imaginary	Imaginary	Real
100	Imaginary	Imaginary	Real
1000	Imaginary	Imaginary	Real
$\kappa \to \infty$	Imaginary	Imaginary	Real

Table 7: Characteristic Roots of the Non-collinear EPs when$\upsilon = 0.7$and $1 < \kappa < \infty$

κ	$\pm\omega_1$	$\pm\omega_2$	$\pm\omega_3$
1.000000001	0.0000547723i	0.999961i	1.00004i
1.00001	0.00547741i	0.996105i	1.00385i
1.01	0.184727i	0.847341i	1.10358i
1.1	Complex	Complex	Imaginary
2	Complex	Complex	Imaginary
5	Imaginary	Imaginary	Real
10	Imaginary	Imaginary	Real
20	Imaginary	Imaginary	Real
50	Imaginary	Imaginary	Real
100	Imaginary	Imaginary	Real
1000	Imaginary	Imaginary	Real
$\kappa \to \infty$	Imaginary	Imaginary	Real

Table 8: Characteristic Roots of the Non-collinear EPs when$\upsilon = 0.9999$and $1 < \kappa < \infty$

κ	$\pm\omega_1$	$\pm\omega_2$	$\pm\omega_3$
1.000000001	0.0000547723i	0.999961i	1.00004i
1.00001	0.00547755i	0.996104i	1.00385i
1.01	0.185321i	0.84646i	1.10416i
1.1	Complex	Complex	Imaginary
2	Real	Imaginary	Real
5	Real	Imaginary	Real
10	Real	Imaginary	Real

20	Real	Imaginary	Real
50	Real	Imaginary	Real
100	Real	Imaginary	Real
1000	Real	Imaginary	Real
$\kappa \to \infty$	Imaginary	Imaginary	Real

From Table 5, It is seen that when$\upsilon = 0.012$and $1 < \kappa < 1.00001$, the six roots are all distinct imaginary roots and the NCEPs is a stable point in this case. When $1.01 \leq \kappa < \infty$, four of the roots are either complex roots or imaginary and the other remaining two roots are real. Therefore, the positive root induces instability at the NCEPs rendering it an unstable equilibrium point. Table 6 gives the roots of characteristic equation (23) of the NCEPs when$\upsilon = 0.3$and$1 < \kappa < \infty$. It is seen that when $1 < \kappa < 1.01$the six roots are all distinct pure imaginary while for $1.01 < \kappa < \infty$four of the roots are either complex roots or imaginary while the remaining two roots are real. The NCEPs is a stable point when $1 < \kappa < 1.01$and unstable when $1.01 < \kappa < \infty$.

Same result follows in the case of Table 7 and Table 8. Hence, we conclude that the–NCEPs is conditionally stable in the entire range of the mass parameter depending on the mass parameter and the parameter kappa. This result differs from those of Hallan and Rana (2001b), Singh and Sandah (2012), Singh and Laraba (2012), Ansari et al. (2019), Abouelmagd et al. (2020), Kaur, et al. (2020, 2021), Kaur and Kumar (2021) and Ansari (2021).

CONCLUSION

The paper investigated the effect of radiation pressure on dynamical structures in the circular Robe's restricted three-body problem (R3BP) with variable masses. The main bodies are assumed to move under the Gylden-Mestschersky problem while their masses vary with time in accordance with the MUL and the second primary is a radiation emitter. The non-autonomous and autonomized equations of the governing dynamical system were deduced under the condition that the first primary has no fluid. Next, the EPs and stability of the autonomized system were studied analytically and numerically.

It was observed that the axial and NCEPs can be stable and unstable depending on the values of the mass parameter, radiation pressure of the second primary and the parameter$\boldsymbol{\kappa}$, which represented the mass variations of the primaries. In the case of the axial EP, the radiation pressure of the second primary reduced the region of stable motion and is therefore a destabilizing force, while the mass variation parameter had both stabilizing and destabilizing effects. The stability of the EPs of the non-autonomous equations was analyzed and it is seen that the solutions do not converge, thereby making the points unstable EPs.

Finally, the ZVCs around the EPs of the autonomized system were explored and it was seen in the case of the axial EP that, the radiation pressure of the second primary decreased the area where motion of the satellite around the axial EP, is permitted, while the mass parameters and the variation constant$\boldsymbol{\kappa}$decreased or increased the region where motion of the satellite around the axial EP is allowed, as they are increased or decreased, respectively. In the case of the NCEPs, it was seen that the radiation of the second primary increased the region where motion of the satellite is allowed, while an increase in the mass parameter and mass variation parameter decreased the region where motion is allowed. The studied formulation can be applied to study small oscillation in the Earth's core of the Earth-Moon system with variable masses, while the EPs may be used in diverse problems of stellar dynamics, and also in other astrophysical and engineering applications.

REFERENCES

Abouelmagd, E. I., Ansari, A. A., Shehata, M. H., (2020). On Robe's restricted problem with a modified Newtonian potential . International Journal of Geometric Methods in Modern Physics. 18,3-19.

Ansari, A. A., Singh, J., Ziyad, A. A., Hafedh B., (2019). Perturbed Robe's CR3BP with viscous force. Astrophysics and Space Science. 364, 95.

Ansari, A.A., (2021). Kind of Robe's restricted problem with heterogeneous irregular primary of N-layers when the outer most layer has viscous fluid. New Astronomy. 83, 101496

Ansari., A, A., Sahdev, S.K., (2022). Variable mass body motion in the perturbed Robe's Configuration. Astronomy Reports. 66, 595-605.

Bekov, A. A., (1988). Libration points of the restricted problem of Three Bodies with variable Mass. Soviet Astronomy Journal. 33, 92-95.

Gelf'gat, B.E., (1973). Current Problems of Celestial Mechanics and Astrodynamics, Nauka, Moscow.

Gylden, H., (1884). Die Bahnbewegungen in EinemSysteme von zweiKörpern in demFalle, dassdieMassenVerNderun-Gen Unterworfen Sind, AstronomischeNachrichten.109, 1-6.

Hallan, P.P. , Rana, N., (2001a). Effect of perturbations in Coriolis and centrifugal forces on the location and stability of the equilibrium point in the Robe's circular restricted three body problem. Planetary and Space Science. 49, 957–960.

Hallan, P.P., Rana, N., (2001b). The existence and stability of equilibrium points in the Robe's restricted three-body problem. Celestial Mechanics and Dynamical Astronomy. 79, 145–155.

Kaur, B., Aggarwal, R., (2012) Robe's problem: its extension to 2+2 bodies. Astrophysics and Space Science. 339, 283–294.

Kaur, B., Kumar. S., Chauchan., S (2020). Effect of perturbations in the Coriolis and centrifugal forces in the Robe-finite straight segment model with arbitrary density parameter Astron Nachr. 341, 32-43.

Kaur, B., Kumar. S., (2021). Stability analysis in the perturbed CRR3BP finite straight segment model under the effect of viscosity. Astrophysics and Space Science. 366, 43 (2021).

Kaur, B., Chauchan., S., Kumar. D., (2021). Outcomes of aspheric primaries in the Robe's circular restricted three-body problem. Applications and Applied Mathematics. 16, 463-480

Kaur, B., Kumar. S., Aggarwal, R., (2022). Effects of viscosity and oblateness on the perturbed Robe's problem with non-spherical primaries. Kinematics and physics of celestial bodies. 38, 248-261

Krasnov, M. L., Kiselyov, A. I., Makarenko, G. I., (1983). A Book of Problems in Ordinary Differential Equations, MIR Publications, Moscow, 255-291.

Leke, O., Ahile, G., (2022). A study on equilibrium points and stability of the Robe's R3BP with density variation. Journal of Applied Physical Science International. 14, 13-41.

Leke, O., Mmaju, C., (2023). Zero velocity curves of a dust grain around equilibrium points under effects of radiation, perturbations and variable Kruger 60. Physics and Astronomy. International Journal. 7, 280-285.

Leke, O., Singh, J., (2023). Out-of-plane equilibrium points of extra-solar planets in the central binaries PSR B1620-26 and Kepler-16 with cluster of material points and variable masses. New Astronomy. 99, 101958

Leke. O., Orum, S., (2024). Motion and zero velocity curves of a dust grain around collinear libration points for the binary IRAS 11472-0800 and G29-38 with a triaxial star and variable masses. New Astronomy. 108, 102177 Elsevier

Leke, O., Amuda, T.O., (2024). Locations of Triangular Equilibrium Points of the Restricted Three-Body Problem with Poynting-Robertson Drag and Variable Masses FUDMA Journal of Sciences. 8, 313-318

Luk'yanov, L. G., (1989). Particular solutions in the restricted problem of three-bodies with variable masses. Astronomical Journal of Academy of Sciences of USSR. 66, 180-187

Mestschersky, I.V., (1902). Ueber die Integration der Bewegungs- gleichungenim Probleme zweierKörper von vernderli- cher Masse, AstronomischeNachrichten. 159, 229-242.

Plastino, A. R., Plastino, A., (1995). Robe's restricted three-body problem revisited. Celestial Mechanics and Dynamical Astronomy. 61, 197–206.

Robe H. A. G., (1977). A new kind of three body problem. Celestial Mechanics. 16, 343–351.

Shrivastava, A.K., Garain, D.N., (1991). Effect of perturbation on the location of libration point in the robe restricted problem of three bodies. Celestial Mechanics and Dynamical Astronomy. 51, 67-73.

Shu Si-hui., Lu Ben-Kui., Chen, Wu-shen., Liu Fu-yao., (2005). A criterion for the stability of the equilibrium points in the perturbed restricted three-body problem and its application in Robe's problem. Chinese Astronomy. 28, 432-440

Singh, J., Leke, O., (2010). Stability of the photogravitational restricted three-body problem with variable masses. Astrophysics and Space Science. 326, 305- 314.

Singh, J., Leke, O., (2012). Equilibrium points and stability in the restricted three- body problem with oblateness and variable masses. Astrophysics and Space Science. 340: 27-41.

Singh, J., Laraba, H.M., (2012). Robe's circular restricted three-body problem under oblate and triaxial primaries. Earth Moon and Planets. 109, 1–11.

Singh, J., Sandah, A.U., (2012). Existence and linear stability of equilibrium points in the Robe's restricted three-body problem with oblateness. Advances in Mathematical Physics. 2012, Article ID 679063, 18 pages.

Singh, J. Leke, O., (2013a). Effects of oblateness, perturbations, radiation and varying masses on the stability of equilibrium points in the restricted three-body problem. Astrophysics and Space Science. 344: 51-61.

Singh, J., Leke, O., (2013b). Existence and stability of equilibrium points in the Robe's restricted three-body problem with variable masses. International Journal of Astronomy and Astrophysics. 3: 113–122.

Singh, J., Leke, O., (2013c). Robe's restricted three-body problem with variable masses and perturbing forces. ISRN Astronomy and Astrophysics. 2013, Article ID 910354.

Singh, J., Omale, J.A., (2014). Robe's circular restricted three-body problem with zonal Harmonics. Astrophysics and Space Science. 353, 89-96 Szebehely, V.G., (1967a). Theory of Orbits. Academic Press, New York.

Taura, J.J., Leke, O., (2022). Derivation of the dynamical equations of motion of the R3BP with variable masses and disk. FUDMA Journal of Sciences. 6, 125- 133.

Wolfram, S., (2015). The Mathematica Book 5th Edition. Wolfram Media, Champaign.

©2024 This is an Open Access article distributed under the terms of the Creative Commons Attribution 4.0 International license viewed via https://creativecommons.org/licenses/by/4.0/ which permits unrestricted use, distribution, and reproduction in any medium, provided the original work is cited appropriately.